

# Kibble-Zurek Mechanism in Microscopic Acoustic Cracking Noises

H.O. GHAFFARI <sup>1(A)</sup>, P. BENSON<sup>2</sup>, K.XIA<sup>1</sup>, R.P.YOUNG <sup>1</sup>

<sup>1</sup> *Department of Civil Engineering and Lassonde Institute, University of Toronto, Toronto, 170 College Street, M5S3E3, ON, Canada*

<sup>2</sup> *Rock Mechanics Laboratory, School of Earth and Environmental Sciences, University of Portsmouth, Burnaby building, Portsmouth, PO1 3QL, UK*

The fast evolution of microstructure is key to understanding “crackling” phenomena [1-5]. It has been proposed [2-3] that formation of a nonlinear zone around a moving crack tip controls the crack tip velocity. Progress in understanding the physics of this critical zone has been limited due to the lack of hard data describing the detailed complex physical processes that occur within. For the first time, we show that the signature of the non-linear elastic zone around a microscopic dynamic crack maps directly to generic phases of acoustic noises, supporting the formation of a strongly weak zone [2-3,5] near the moving crack tips. We additionally show that the rate of traversing to non-linear zone controls the rate of weakening, i.e. speed of global rupture propagation. We measure the power-law dependence of nonlinear zone size on the traversing rate, and show that our observations are in agreement with the Kibble-Zurek mechanism (KZM) [8-9].

The spatio-temporal evolution of acoustic signals, known as crackling noise [1], is a direct result of failing bonds during the fracture of materials in the brittle regime. Such signals, if properly interpreted, may be used to better understand the detail of rupture progress in the vicinity of rupture tips under a broad range of scales and conditions [2-4]. During cracking, part of the energy stored in the crack tip is transformed into breaking molecular and atomic bonds, resulting in new crack surface(s). The key to understanding the cracking process lies in the structure of the near-tip region, where stresses become so large. Due to the microscopic size and near-sound speed velocity of the near-tip zone, direct measurements are very difficult, with numeric or atomistic calculations being the only means to analysis it [5]. Because of the large strains that always exist near a crack’s tip, nonlinear elastic contributions must occur. Recent numerical progress [2-3] suggests that a non-linear zone around any moving crack tip governs the rupture velocity. Further, investigating slow cracks in gels [5] show that the spatial complexity of energy flow into the rupture tip closely maps to

the curvature of the tip, resulting in deviation of the curvature of tip from linear elastic analyses that are commonly used in material science.

In this study we use functional networks applied to multi-stationary acoustic emission records from microscopic cracks of rock deformation and rock friction experiments (see methods section) to show that the nucleation phase of micro-ruptures reflects signatures of non-linearity (i.e., a critical or impulse zone), which allows an independent verification of the rupture state. We illustrate how the initial strengthening phase acts as a barrier against the eventual dynamic failure during rock deformation, and that the details of evolution during this stage, of only a few microseconds duration, plays a major role in determining the final rupture state. Our observations indicate that cracking noises which traverse faster to their critical point induce a higher magnitude of material softening, reducing the weakening rate. These new results facilitate prediction of the ongoing rupture state and its magnitude, and are consistent with other studies [6-7]. For the first time, we show that cracking noises hold the signature of Kibble-Zurek mechanism (KZM) [8-11] that provides an estimation of microscopic defect density versus traversing rate to critical zone. A key result of KZM relates faster “quenches” to shorter freeze-in time and higher defect densities. This proves that dynamics of topological defects in near tip region likely follows universality of continuous phase transitions. In addition, we illustrate that cracks exhibiting global rupture fronts with velocity faster than Rayleigh waves (i.e., super-shear rupture fronts [13]) display a complex configuration of non-linear zone prior to the fast weakening phase.

## Results

We use short-term records of multi-stationary acoustic emission waveforms from rock deformation experiments under different confining pressures and loading paths on two rock types: Westerly granite and Basalt from Mount Etna, Italy. (datasets Lab.EQ1, Lab.EQ2, Lab.EQ3 and Lab.EQ4 - see methods section and supporting information). We apply tools from the theory of complex networks to analysis microscopic cracks with the received AE waveforms [4,12]. These results then allow us to develop a new interpretation of multiple acoustic-crackling signals involving micro-second evolution of different regimes of dynamic “defect”, encoded in “*Q-profiles*” (a temporal modularity of constructed functional networks). The analysis proceeds as follows (Fig.1a-Fig.S1):

S-phase: an initial strengthening or nucleation regime with fast-approaching to the main critical point or the catastrophic failure phase; W-phase: a fast-slip or weakening phase; D-phase: a slow slip phase (decelerating phase) [12,14-15]. To better understand the S-phase, we use the reciprocal of modularity profiles (R-profiles) which closely resembles dynamic stress profiles (Fig.S1).

To investigate the nucleation phase of dynamic cracks (and defects), we employed these laboratory tools in combination with a definition of the critical zone onset,  $R_c$ , as a step change in curvature in the computed R-profile (Fig.2 b,c). Defining a critical zone (hereafter, C-zone), which is accompanied by a very fast transition to negative  $\frac{\partial^2 R}{\partial t^2}$ , as well as impulse trend in reciprocal of local energy flow in functional networks, (Fig.2 and methods section). As illustrated in Fig.2, two main impulsive signals are recorded in the R-profiles: one before  $R_{\max}$  and the second in the second evolutionary phase subsequent to it. The duration of the C-zone in the first phase for most of the cases are nearly equal to its second portion, displaying a symmetric impulse zone (Fig.2). We define the duration of C-zone  $\tau_c$  as the onset time of critical zone (i.e., impulse zone) to the time of maximum R(t). Further, we define “sharpness degree (Fig.2c) as  $\zeta \equiv ((\frac{\partial^2 R}{\partial t^2})_{\max} - (\frac{\partial^2 R}{\partial t^2})_{\min})$  which correlates with the local rate of ramping (Fig.S6), and show that it controls the rate of weakening where the fast-slip occurs (Fig.3c and Fig.S3). This is illustrated in Fig 3c, as traverses across to the C-zone increase in speed, a slower rate of weakening is observed. We interpret this key result as the effect of higher C-zone size (Fig.3a), which generates a slower weakening rate due to a slower global rupture front. This finding implies that earlier onset of C-zone associates with smaller  $\zeta$  and then higher rupture velocity. This observation is in agreement with Buehler’s molecular dynamic simulations [2] regarding inverse scaling of the onset of non-linear zone and crack velocity. This evidence further promotes our hypothesis that the initial strengthening phase acts as an obstacle and that the “path” of the system in crossing from an impulsive zone to a more benign zone is the key to determine the next evolutionary phases in acoustic excitations.

Fig.3b shows that a shorter C-zone scales inversely with faster traversing to C-zone. This finding indicates that the time to freeze out defects is strongly associated with the rate of transitioning to this regime, implying an active Kibble-Zurek mechanism (KZM) [9-11]. Based on this theory, the resulting density of defects left behind by transitions is dependent on the rate at which the critical

point is traversed, and the rate with which the systems can adjust (i.e., healing time). This mechanism is reflected in the density of defects and freeze-out time which is scaled with ramp rate [10-11]. Based on our new data, the traversing rate to the C-zone is scaled as (Fig.S6) :  $\zeta \sim \left(\frac{dR_c}{dt}\right)^{1.2}$  and using  $\Delta R \sim \zeta^{0.5}$  (Fig.4a-inset) ,we now have  $\Delta R \sim \left(\frac{dR_c}{dt}\right)^{0.6}$ . Here  $\Delta R = R_{\max} - R_c$  is proportional to the size of softening or non-linear zone (i.e., density of excitations) and  $\frac{dR_c}{dt}$  is the rate of the ramping (Fig.2-also see SI for further discussion). The predicted exponent by mean-filed theory is 0.5 [10] compared with the renormalization group of 0.66. The agreement of the exponents and trend of freeze-out time with the rate of transition is in excellent agreement of the Kibble-Zurek mechanism in the scale of microscopic cracking noises.

Further investigation of acoustic excitation events shows two typical behaviours in their critical zone. While most of the events imprint uniform evolution of C-zone, some events display a complex trend of this zone. To further understand the nature these unusual events, we calculated the C-zones from super-shear and sub-shear macro-ruptures reported in [22] (Fig.4). Whilst reference to super-shear events such as these produce a complex C-zone, including significant fluctuations within this zone (Fig.4, Fig.S9-12), sub-shear events reflect simpler evolutionary trends within this zone. As such, we have shown in this work that key changes in the curvature of C-zone are correlated with very fast rupture events. By fitting a polynomial functions on the C-zone, we are able to describe both sub-shear (i.e. regular earthquakes) and super-shear events with polynomial function of degree 2 and 3 (or higher for super ruptures) respectively (Fig. 5 and Fig.S.12-S.13). As a result, we interpret the observed stiffening regime in C- zone of microscopic events with very fast ruptures where the rupture velocity approaches intersonic speeds. These observations resemble the results of molecular dynamic models in which elastic stiffening or softening elastic behaviour is induced through disharmonic interatomic potential, producing super-ruptures and sub-Rayleigh fronts respectively [2]. Further analysis of events from our experiments indicates that extreme fluctuation in the critical zone is not limited to macro-scale events and can be accessible in micro-scales (Fig.5 and Fig.S.11-S.12). In such cases, and by using the same characteristics of C-zone in macro-scale template events, we postulate that some of microscopic events in rock interfaces possess the signature of super shear events. The reason for such microscopic super-shear events lies in the build-up of large stresses at

microscopic scales, which may reach to the required order of stress to onset super ruptures in microscopic damage zones [16]. This is the first indication for the occurrence of super shear defects in microscopic scale and proves the results of atomistic models concerning rupture (or dislocation) velocities.

To conclude, we have shown, for the first time via laboratory data, the effect, of a few microseconds duration, of fracture evolution derived purely from microscopic defects using multiple acoustic excitations. This was used to define the rupture regime (style) and the rupture dimension. We found that acoustic waveforms may be analyzed via mathematical graph theory to yield new insight on the structure of dynamic crack-tip processes, confirming the recent approaches on the role of non-linear zones to govern the rupture state. For the first time, we confirmed the validation of KZM mechanism in the scale of microscopic cracks and acoustic-crackling noises, where the size of non-linear critical zone is scaled with the traversing rate to this zone. For supershear ruptures, we found that complexity in the nucleation phase induces a stiffening zone in vicinity of moving crack tip. With using such characteristics of C-zone, we recognized microscopic super rupture events in laboratory tests; a significant step towards recognizing dislocations with velocity faster than shear waves.

## Methods

**Laboratory Procedures:** We use four sets of recorded acoustic emissions-labeled as Lab.EQ1, 2 , 3 and 4 -from Westerly granite and Basalt rock samples (most of the analyzed events are precursor rupture fronts). The Lab.EQ1and 2 are the recorded multi-stationary acoustic waveforms from evolution of frictional rock-interfaces of Westerly Granite samples. The interfaces were in dry conditions with smooth (saw-cut) and naturally -rough surfaces, respectively [17]. The evaluated events are from different stages and position and then are not limited to particular stage of the tests. The Lab.EQ3 is the fast-loading experiment on a cylindrical sample of Westerly Granite ( $\sim 10^{-5} \text{ s}^{-1}$ ) at 50MPa confining stress, which is about an order faster than Lab.EQ1 and 2 [18]. Lab.EQ4 are events from Basalt samples; described in [19].The global loading rate was about  $10^{-6} \text{ s}^{-1}$ . We also use unamplified waves with definite global rupture velocity in centimeter scales from [22] as our macroscopic template events. We use these template events to discover microscopic super-shear events. In all of the above experiments, we reordered amplified events using 16 to 18 sensor networks in both short (discrete events) and long timescale recorders (AE records).

**Networks of Acoustic emission waveforms:** The idea in studying each single acoustic excitation event is to determine the onset of the critical phase where the defects (damage) precipitate out in a matrix of elastic material. The details of the employed algorithm can be found in [4, 12, 14]. In summary, the algorithm uses a thresholded-closeness metric to establish *functional networks* where the nodes are the sensors and per each time step in a short-time interval ( $\sim 200\mu\text{s}$ ), a network is assigned. Per each network a set of properties, including modularity index are extracted. The temporal evolution of Q values in the monitored time interval forms Q-curves. Q(t) carries generic universal time scales,

distinguishing microseconds details of micro-cracks. Regarding wide range applications of acoustic emissions and their observation in an unusually large number of experiments, finding such a universal frame on complicated emitted waveforms are much of important. Following [4,14], we found three generic classes, corresponding to the following phases in Q-profiles (Fig.S.1) : (1) S-phase: nucleation and main deformation phase with the signature of initial strengthening (2) W-phase or fast-slip and (3)D-phase or slow slip stage. To distinguish the role of S- phase, we define a parameter such as  $R$ :  $R \equiv (Q_{norm.})^{-1}$  where  $Q_{norm.} = \frac{Q}{Q_0}$  ( $Q_0$  is the initial or rest value of  $Q(t)$ ). The trend of  $R(t)$  is similar to

the temporal trend of maximum of node's degree (Fig.S.3). We also use a parameter indicating the mean of local energy flow for a given network: betweenness centrality (B.C). It characterizes the importance of a node using the number of

shortest paths from all nodes that pass through that node [20]. We discover that negative concavity of  $\frac{\partial^2 R}{\partial t^2}$  is reflected in negative portion of  $\log \langle B.C \rangle$ , where  $\langle \dots \rangle$  indicates spatial average over nodes. These techniques closely support the theory of accelerated waves in incipient plasticity in crystals (see SI-section3) [21].

## Supplementary Information

Supplementary information accompanies this paper.

## Acknowledgements

We would like to acknowledge and thank B.D. Thompson (Mine Design Engineering, Kingston, Canada), A.Schubnel (Laboratoire de Géologie de l'Ecole normale supérieure, France), S.Nielson (Istituto Nazionale di Geofisica e Vulcanologia (INGV) for providing part of the employed data set in this work. The first author would like to acknowledge Ekhard Salje, Adolfo del Campo for their encouragements and points on the manuscript.

## Author Contributions

All authors contributed to the analysis and writing of the manuscript.

## Competing interests statement

The authors declare no competing financial interests.

## References

- [1] Sethna, J. P., Dahmen, K. A., & Myers, C. R. (2001). Crackling noise. *Nature*, 410(6825), 242-250.
- [2] Buehler, M. J., Abraham, F. F., & Gao, H. (2003). Hyperelasticity governs dynamic fracture at a critical length scale. *Nature*, 426(6963), 141-146.

[3] Buehler, M. J., & Gao, H. (2006). Dynamical fracture instabilities due to local hyperelasticity at crack tips. *Nature*, 439(7074), 307-310.

[4] Ghaffari, H. O., & Young, R. P. (2013). Acoustic-friction networks and the evolution of precursor rupture fronts in laboratory earthquakes. *Scientific reports*, 3.

[5] Livne, A., Bouchbinder, E., Svetlizky, I., & Fineberg, J. (2010). The near-tip fields of fast cracks. *Science*, 327(5971), 1359-1363.

[6] Ellsworth, W. L. & Beroza, G. C. Seismic evidence for an earthquake nucleation phase. *Science* 268, 851–855 (1995).

[7] Olson, E. & Allen, R. M. The deterministic nature of earthquake rupture. *Nature* 438, 212–215 (2005).

[8] Kibble, T. W. B. Topology of cosmic domains and strings. *J. Phys. A: Math. Gen.* 9, 1387–1398 (1976).

[9] Zurek, W. H. Cosmological experiments in superfluid helium? *Nature* 317, 505–508 (1985).

[10] del Campo, A., & Zurek, W. H. (2014). Universality of phase transition dynamics: Topological defects from symmetry breaking. *International Journal of Modern Physics A*, 29(08).

[11] Pyka, K., Keller, J., Partner, H. L., Nigmatullin, R., Burgermeister, T., Meier, D. M., ... & Mehlstäubler, T. E. (2013). Topological defect formation and spontaneous symmetry breaking in ion Coulomb crystals. *Nature communications*, 4.

[12] Ghaffari, H. O., Thompson, B. D., & Young, R. P. (2014). Complex networks and waveforms from acoustic emissions in laboratory earthquakes. *Nonlinear Processes in Geophysics*, 21(4), 763-775.

[13] Xia, K., Rosakis, A. J., & Kanamori, H. (2004). Laboratory earthquakes: The sub-Rayleigh-to-supershear rupture transition. *Science*, 303(5665), 1859-1861.

[14] Ghaffari, H. O., Nasseri, M. H. B., & Young, R. P. (2014). Faulting of Rocks in a Three-Dimensional Stress Field by Micro-Anticracks. *Scientific reports*, 4.

[15] Ben-David, O., Rubinstein, S. & Fineberg, J. Slip-Stick: The evolution of frictional strength. *Nature*. 463, 76 (2010).

[16] Gumbsch, P., & Gao, H. (1999). Dislocations faster than the speed of sound. *Science*, 283(5404), 965-968.

[17] Thompson, B. D., Young, R. P. & Lockner, D. A. Premonitory acoustic emissions and stick-slip in natural and smooth-faulted Westerly granite. *J Geophys Res.* 114, B02205J (2009).

[18] Thompson, B. D., Young, R. P., & Lockner, D. A. (2006). Fracture in Westerly granite under AE feedback and constant strain rate loading: nucleation, quasi-static propagation, and the transition to unstable fracture propagation. In *Rock Damage and Fluid Transport, Part I* (pp. 995-1019). Birkhäuser Basel.

[19] Benson, P. M., Vinciguerra, S., Meredith, P. G., & Young, R. P. (2010). Spatio-temporal evolution of volcano seismicity: A laboratory study. *Earth and Planetary Science Letters*, 297(1), 315-323.

[20] Newman, M. E. J. *Networks: An Introduction* (Oxford University Press, 2010).

[21] Li, J., Van Vliet, K. J., Zhu, T., Yip, S., & Suresh, S. (2002). Atomistic mechanisms governing elastic limit and incipient plasticity in crystals. *Nature*, 418(6895), 307-310.

[22] Schubnel, A., Nielsen, S., Taddeucci, J., Vinciguerra, S., & Rao, S. (2011). Photo-acoustic study of subshear and supershear ruptures in the laboratory. *Earth and Planetary Science Letters*, 308(3), 424-432.

## Figures

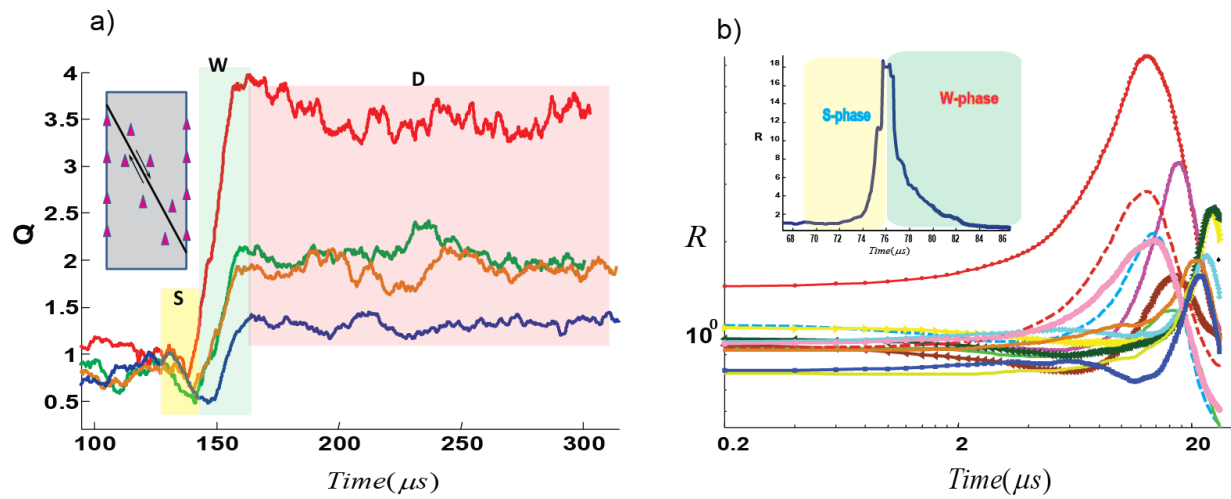


**Figure 1 | Study of nucleation phase of microscopic failures** (a) Three main stage of typical acoustic crackling noises in normalized Q-profiles :S-W-D phases correspond with strengthening, weakening and decelerating stages, respectively. The inset shows schematic representation of Lab.EQ1(saw-cut fault) with mounted acoustic sensors (red triangles) (b) Typical R- profiles in log-log plot from Lab.EQ1 ; Inset: nucleation (S-phase) and weakening regimes (W-phase).

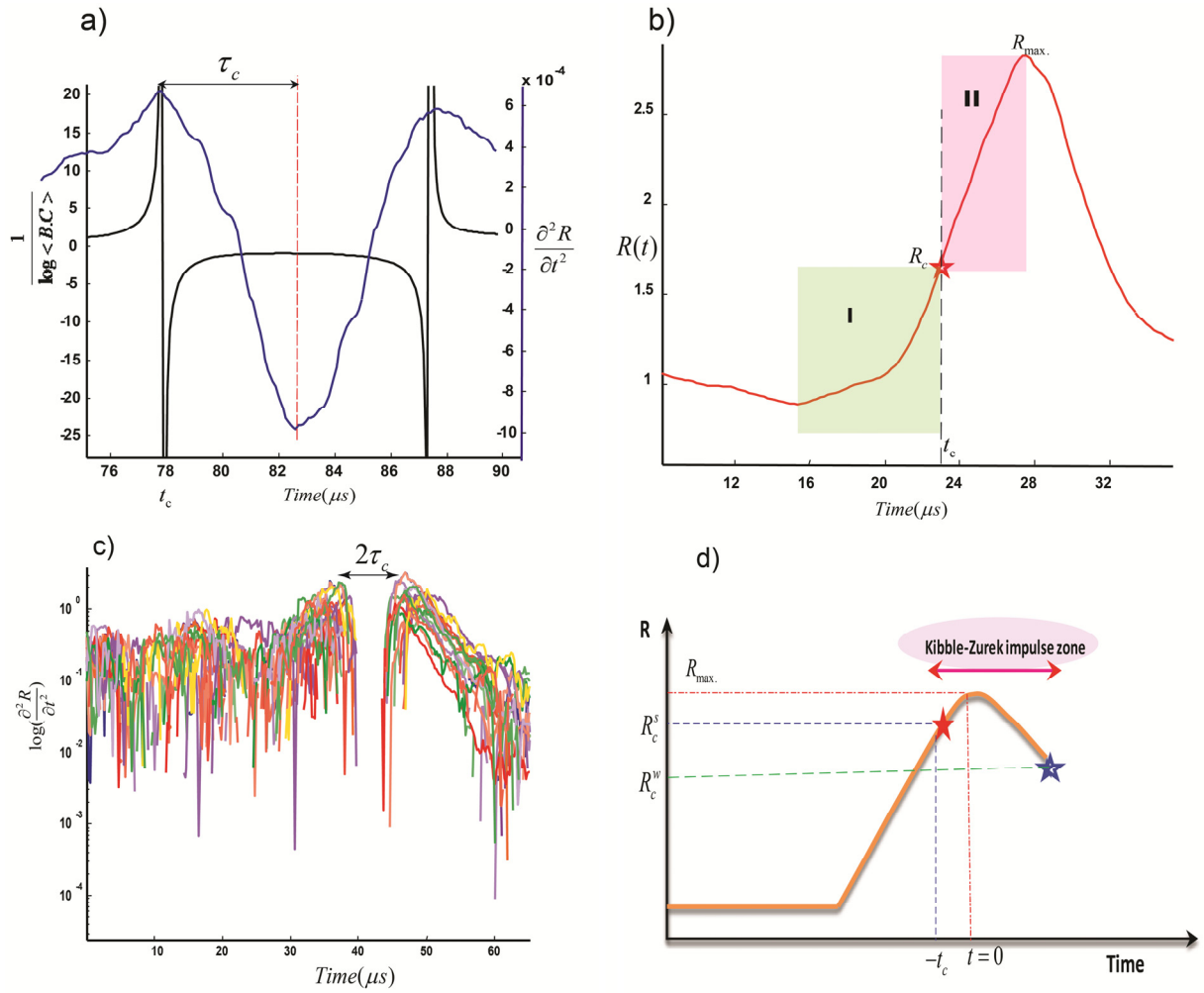


**Figure 2| Critical zone and onset of instability in emitted waves.** (a) Inverse of betweenness centrality (B.C) is used as a criterion to define the onset of critical zone. (b) Approaching the critical point corresponds to drastic change in the curvature of R-profile. Duration of C-zone is defined as  $\tau_c$ . S-phase includes two sub-stages: ramping period (stage I) and C-zone (stage II); (c) C-zone is defined with a clear gap in the logarithmic representation of  $\frac{\partial^2 R}{\partial t^2}$  (profiles from Lab.EQ2). (d) Schematic representation of the quenching process, where  $t=0$  is the threshold for the onset of weakening and the freezing dynamics occurs in the interval  $[R_c^s, R_c^w]$ . We assume symmetric impulse zone:  $R_c^s \approx R_c^w \equiv R_c$ .

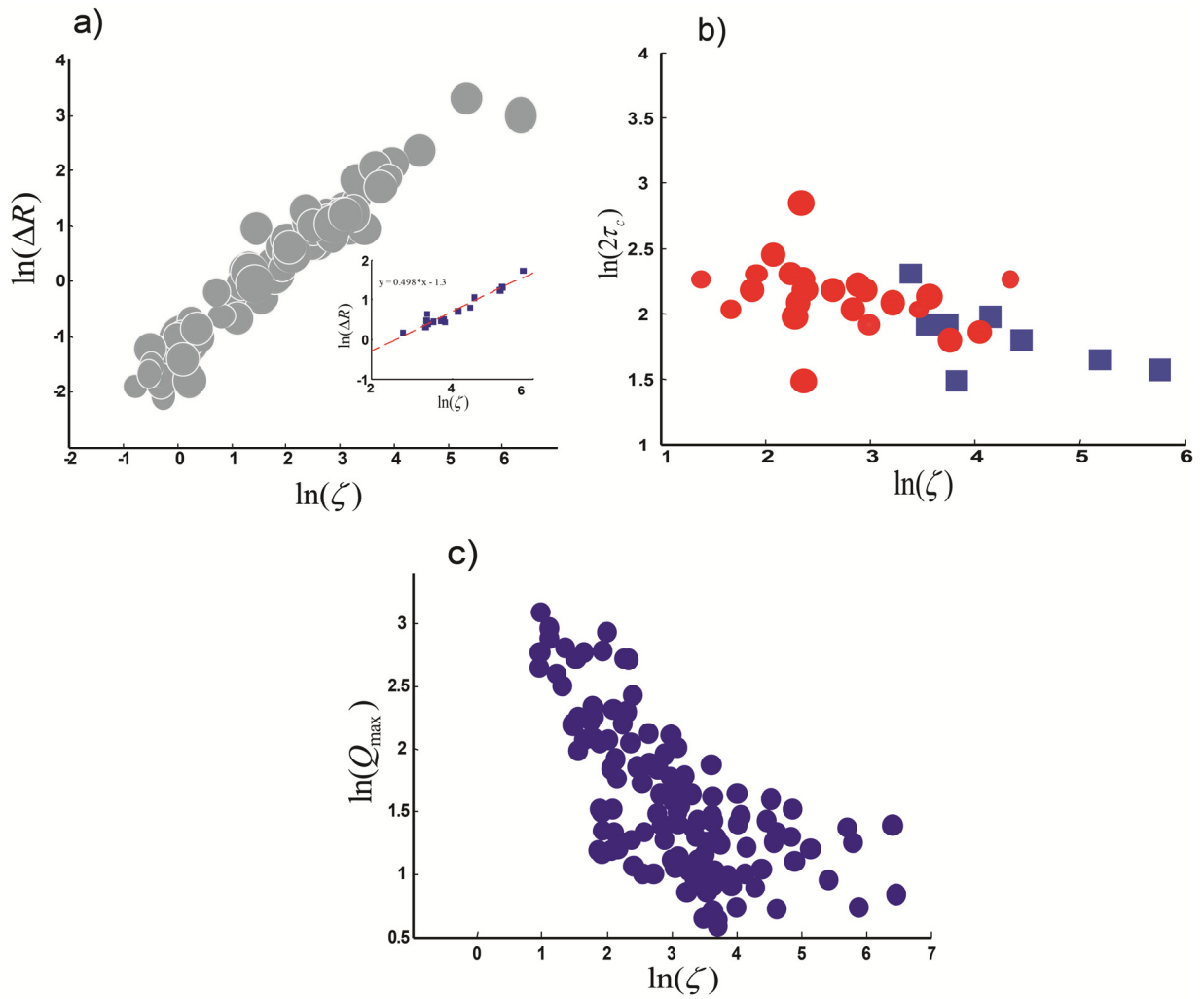


**Figure 3| Study on C-zone.** (a) Ruptures with sharper transition ( $\zeta$ ) to critical regime induce greater C-zone size (proportional to  $\Delta R = R_{\max} - R_c$ ). We have shown typical rupture fronts from Lab.EQ3. The sharpness degree is defined as  $\zeta = 1000 \times ((\frac{\partial^2 R}{\partial t^2})_{\max} - (\frac{\partial^2 R}{\partial t^2})_{\min})$ . Inset: scaling of the softening zone with smoothness degree (Lab.EQ2):  $\Delta R \sim \zeta^{0.5}$ . (b) The faster traversing to C-zone shrinks the duration of freeze-out time ( $\tau_c$  in  $\mu\text{s}$ ). The data sets are from Lab.EQ (1-red) and Lab.EQ(2-blue). (c) Memory effect in fast-weakening regime: Events with faster weakening rate scale with smoother transition to C- zone. We have shown *log-log* plot of the maximum modularity index ( $Q_{\max}$ ) observed as a function of sharpness degree (events from Lab.EQ3). Also see Fig.S.5-S.8.

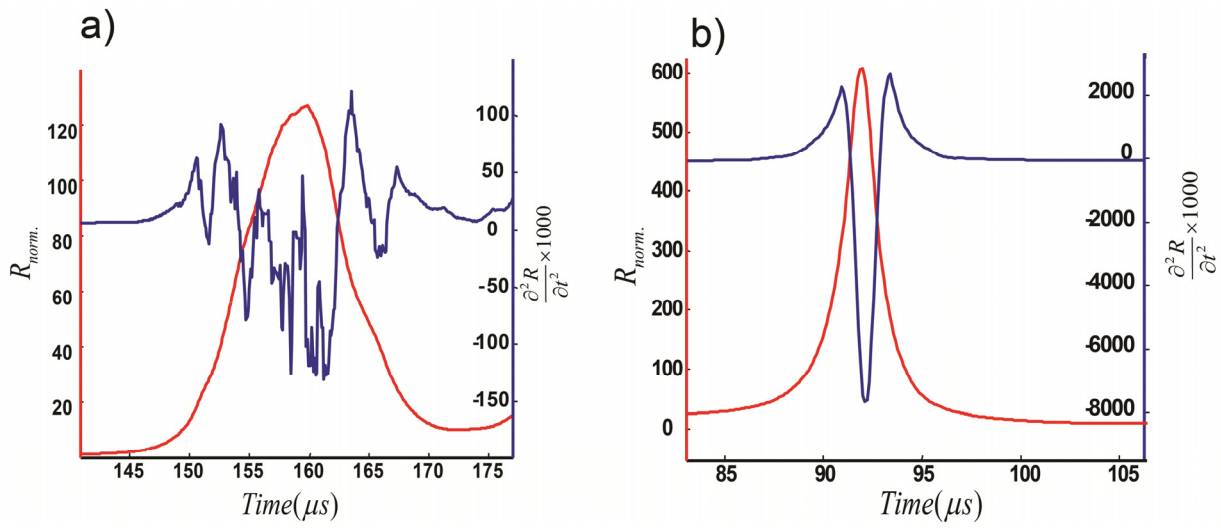
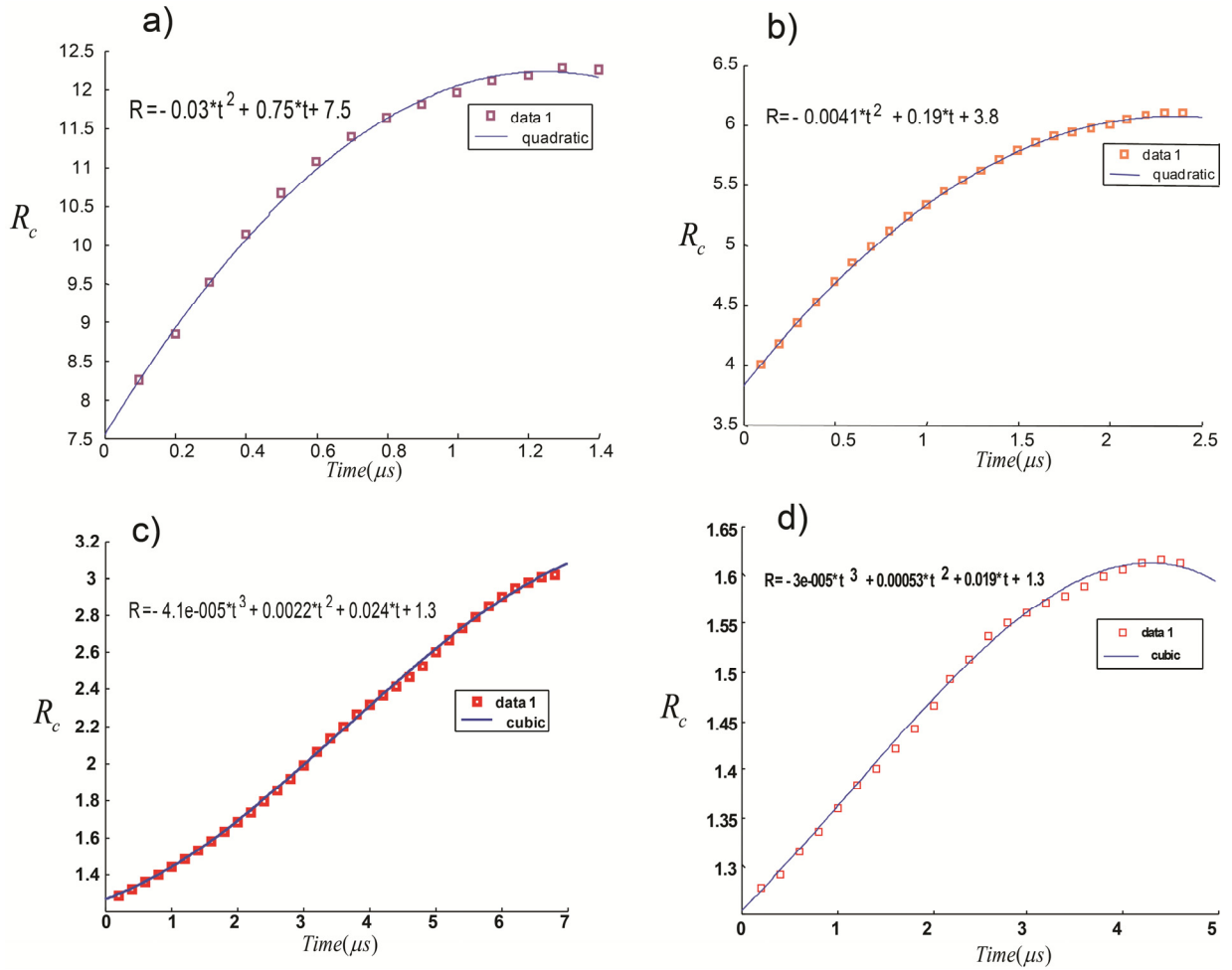


Figure 4| Critical zone in sub-shear and super shear cracks. (a) A typical super-shear crack is associated with relatively long -complex critical zone and smoother curvature while (b) sub-shear crack imprints a simple C-zone with sharp transition to this regime (also see Figs.S9-S13).  $R_{norm.}$  is normalized  $R(t)$  to the initial rest value.



**Figure 5 | microscopic sub-shear and super-shear events** (a-b) microscopic sub-shear acoustic emission events display typical quadric polynomial pre-peak function. Here we have shown microscopic events from Lab.EQ4 with a fitted second order polynomial function on C-zone . The duration of C-zone –in these examples- are between 1.4 and 2.5 $\mu$ s. (c-d) The first observation of microscopic super-shear defects with relatively longer duration of C-zone with cubic term in pre-peak function of  $R(t)$  (events from Lab.EQ2). Also see Fig.S12-S.13.